



Original Research Paper

On the enhancement of particle deposition in turbulent channel airflow by a ribbed wall



C.D. Dritselis

Department of Mechanical Engineering, University of Thessaly, Pedion Areos, 38334 Volos, Greece

ARTICLE INFO

Article history:

Received 26 August 2016

Received in revised form 24 November 2016

Accepted 22 December 2016

Available online 3 January 2017

Keywords:

Particle deposition

Surface ribs

CFD

Large-eddy simulation

Lagrangian particle-tracking

ABSTRACT

The particle deposition at a vertical wall roughened by transverse square bars placed at a small spacing between them is investigated using large-eddy simulation of the turbulent flow in a ribbed channel with the gravity aligned in the flow direction together with Lagrangian particle-tracking. It is found that the particle deposition coefficient is substantially increased in the presence of roughness elements, exhibiting a weaker dependence on the variation of particle response time relative to the case of smooth channel. The enhancement ratio of particle deposition varies from three for the larger size particles to about 400 for the smaller particles examined here. The friction-weighted enhancement ratio of particle deposition is higher than unity for all particle sets, indicating that the present ribbed channel configuration efficiently increases particle deposition with respect to the increase in energy losses. The rise in the particle deposition coefficient at the rough surface is closely related to the direct inertial impaction and interception mechanisms. The population of particles depositing at the rear surface of the square bars is very small, revealing that an enlargement of the effective deposition area is not necessarily translated to a similar augmentation of particle removal.

© 2016 The Society of Powder Technology Japan. Published by Elsevier B.V. and The Society of Powder Technology Japan. All rights reserved.

1. Introduction

Several human health problems associated with heating, ventilation, and air conditioning (HVAC) systems are caused by the pollution of ventilation ducts. Particle deposition onto duct surfaces is a critical factor, which influences size distributions, concentrations, and fate of indoor aerosols. Re-suspension of the deposited particles in a ventilation duct may also take place, resulting in polluted indoor environment and adverse health effect. It has been found that the removal of particles is significantly increased by a rough wall consisting of elements with various sizes and shapes placed on the solid surface in various arrangements and combinations, improving the collection efficiency of electrostatic precipitators [1] and the air filtration in ventilation ducts [2–4]. However, the total energy losses are usually increased in such geometric configurations, and the trade-offs between those losses and particle removal need to be clarified. Therefore, it is important to advance our knowledge and understanding of the complicated processes occurring in particulate flows and particularly in particle deposition on rough surfaces, in order to maintain and improve indoor air quality (IAQ).

Relatively few studies have been performed on the particle deposition enhancement by a rough wall. The effect of surface roughness on the particle deposition has been quantified in several experimental works by using irregular size materials or well-defined large scale obstructions [2–5]. Particle deposition was measured rather indirectly by calculating the particle mass rate, while certain details were not provided. Nevertheless, all these works indicate that the amount of particles depositing on rough walls is higher than that on smooth walls. Moreover, the significance of the interception mechanism for the augmentation of particle deposition observed at the rough walls is clearly highlighted.

Several aspects of the transport and deposition of aerosol particles in turbulent channel flows with surface ribs have been investigated mostly based on Reynolds-averaged Navier-Stokes (RANS) models together with Lagrangian particle-tracking [6–12]. In accordance with the experimental observations, the numerical studies predict an increase of particle deposition at the rough surface. The differences in the dynamic behavior between spherical and cylindrical particles in a channel flow with one surface rib were discussed by Lo Iacono et al. [13], who used large-eddy simulation (LES) coupled with Lagrangian particle-tracking. They showed that spherical particles were concentrated mostly at the frontal surface of the rib, while cylindrical particles didn't exhibit

E-mail address: dritseli@mie.uth.gr

Nomenclature

A_d	deposition area	$u_{p,i}^n$	velocity of the n particle
C	LES parameter	U_{rms} , V_{rms} , and W_{rms}	non-dimensional rms fluid velocity fluctuations in the x , y , and z directions, respectively
c_D	drag coefficient		
C_f	viscous shear stress		
d_p	particle diameter	$u_{\tau,0}$	wall friction velocity at $w/k = 0$
f	friction factor	U_τ	non-dimensional wall friction velocity
$f_{D,i}^n$	drag force acting on particle	W	cavity width
F_d	friction drag	\mathbf{X}	unit vector in the x -direction
f_G	gravity force acting on particle	$x(X), y(Y)$, and $z(Z)$	coordinates (non-dimensional) in the streamwise, wall-normal and spanwise direction, respectively
Fr	Froude number	$X_u(nbl), X_l(nbl), Y_{in}, Y_{out}$	planes of the upper and lower horizontal surfaces of the nbl square bar and planes of the inner and outer vertical surfaces of the rough wall, respectively
f_{rough}	friction factor of the rough channel		
f_{smooth}	friction factor of the smooth wall	$x_{pc,i}^n$	particle position at contact with the planes of the rough wall
g	gravity	$x_{p,i}^n$	particle position
h	half distance between the right smooth wall and the crest of the left rough wall	y^+	non-dimensional distance
k	dimension of the square bar	y_0^+	origin of distribution of correction 2
k_d^+	normalized particle deposition coefficient		
l	distance from the vertical crests of the rough wall		
L_{ij}	LES quantity		
L_x , L_y , and L_z	dimension of the channel in the streamwise, wall-normal and spanwise direction, respectively		
M_{ij}	LES quantity		
m_p	the spherical particle mass		
\mathbf{n}	unit vector normal to the wall contour		
n_d	number of deposited particles		
$n_{\delta V}$	initial number of particles		
\bar{p}	pressure		
\bar{P}	non-dimensional pressure		
P_d	form drag		
Re	Reynolds number		
Re_p	particle Reynolds number		
\mathbf{s}	unit vector parallel to the wall contour		
$\bar{\mathcal{S}}_{ij}$	resolved strain-rate tensor		
$ \bar{\mathcal{S}} $	magnitude of resolved strain-rate tensor		
S_{pf}	particle-fluid density ratio		
St^*	non-dimensional particle response time		
t , T	time (non-dimensional)		
t_c	contact time		
\bar{U}_i	component of the filtered velocity in the i -direction		
\bar{U}_i	non-dimensional component of the filtered velocity in the i -direction		
$\tilde{u}_{\text{p},i}^n$	undisturbed fluid velocity at the particle position		
\bar{U}	mean fluid velocity in the streamwise direction		
u_b	bulk velocity		
$U_{p,d}$, $V_{p,d}$, and $W_{p,d}$	non-dimensional components of the wall-impact velocity in the x , y , and z directions, respectively		

such tendency. Lo Iacono et al. [14] showed that the mass-sink concept could be employed in engineering practice, even though it could not capture the microphysics of the interaction of the suspended particles with the roughness element. The effect of the sub-grid scale fluid motions on the particle trajectories in turbulent channel flows with one surface rib was investigated by Khan et al. [15]. They concluded that their effect is rather small on the motion of particles with high response times in well-resolved LESs. On the other hand, the model impact could be non-negligible at different flow regimes, such as higher Reynolds number of the flow, insufficient grid resolution, and/or low particle inertia.

In the present study, the effect of roughness elements on the particle deposition is investigated by using LES of the downward turbulent flow in a vertical channel with one wall consisting of square bars separated by a cavity, as shown in Fig. 1. The combination of numerical methods (LES/immersed boundary method/

			Greek
			Γ enhancement ratio of particle deposition
			Δ characteristic length scale
			δ_{ij} Kronecker delta
			δt_d time interval
			δV volume
			Δx , Δy , and Δz grid spacing in the x -, y -, and z -directions, respectively
			η friction-weighted enhancement ratio of particle deposition
			λ streamwise wavelength
			ν air kinematic viscosity
			Π extra pressure gradient
			ρ_f air density
			ρ_p particle density
			τ_{ij}^r subgrid scale stress tensor
			τ_p particle relaxation time
			τ_w wall stress
			Symbols
	$\bar{}$	filtered LES quantities	
	\wedge	variables calculated on a test filter	
	$\langle \rangle_{z,t}$	denotes averaging over the z -direction and time	

Lagrangian particle-tracking) has not been utilized previously for the in depth investigation of particle deposition enhancement by a rough wall, which so far is based on RANS simulations. This work differs from previous LES studies [13,14] in several aspects, as for example, in the size and arrangement of roughness elements, the Reynolds number of the airflow, the gravity orientation, and the particle response time, indicating that a different parameter space is examined here. Moreover, the main objective of this work is focused on addressing the impact of square bars on the particle deposition enhancement and quantifying it properly based on measures, such as the deposition enhancement ratio and the friction-weighted efficiency factor. To the best of the author's knowledge, this is performed for the first time by using LES results. LES can provide a reliable representation of the turbulent flow fields, and several quantities required for the description of particle deposition onto rough walls can be obtained accurately, such as

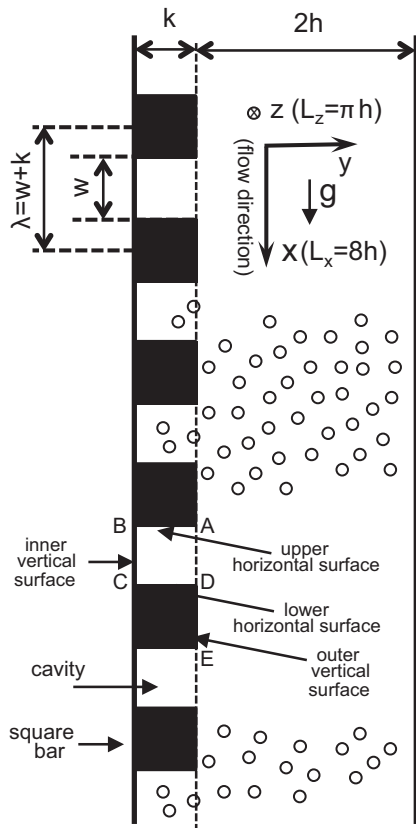


Fig. 1. Flow configuration.

the wall friction velocity, the friction drag and the form drag. The turbulent airflow is then used to determine the particle motion and estimate deposition rates. Except for their theoretical value, the results shown here can serve also as a guide for engineering applications and designs.

2. Numerical models and methodology

2.1. Turbulent airflow model

The configuration of the particle-laden flows under investigation is shown in Fig. 1. No-slip boundary conditions are imposed for the velocity at the channel walls (y -direction), while periodic boundary conditions are applied to the dependent variables in the streamwise (x) and spanwise (z) directions. In LES, the instantaneous turbulent velocity of the carrier phase is decomposed into a component representing the large flow scales and a second one that corresponds to the small scales of the turbulent flow. The LES equations are obtained by filtering the continuity and Navier–Stokes equations. The three-dimensional (3d), unsteady, incompressible filtered continuity and Navier–Stokes equations governing the present turbulent airflow are

$$\frac{\partial \bar{u}_i}{\partial x_i} = 0, \quad (1)$$

$$\frac{\partial \bar{u}_i}{\partial t} + \frac{\partial \bar{u}_i \bar{u}_j}{\partial x_j} = -\frac{1}{\rho_f} \frac{\partial \bar{p}}{\partial x_i} + \nu \frac{\partial^2 \bar{u}_i}{\partial x_j \partial x_j} - \frac{\partial \tau_{ij}^r}{\partial x_j} + \Pi \delta_{ii}, \quad (2)$$

where \bar{u}_i is the component of the filtered velocity in the i -direction, \bar{p} is the pressure, ρ_f and ν are the air density and its kinematic viscosity, respectively, and the overbar indicates filtered LES quantities. The effect of the subgrid scale motions on the grid scale

velocities of the carrier phase is taken into account by the term τ_{ij}^r , which is modeled as

$$\tau_{ij}^r = \bar{u}_i \bar{u}_j - \bar{u}_i \bar{u}_j = -2C\bar{\Delta}^2 |\bar{S}| \bar{S}_{ij}, \quad (3)$$

where \bar{S}_{ij} is the resolved strain-rate tensor and $|\bar{S}| = (2\bar{S}_{ij}\bar{S}_{ij})^{1/2}$ its magnitude. In Eq. (3), $\bar{\Delta}$ is a characteristic length scale given by $\bar{\Delta} = (\Delta x \Delta y \Delta z)^{1/3}$, where Δx , Δy , and Δz are the grid spacings in the x -, y -, and z -directions, respectively. The parameter C is determined based on the dynamic Smagorinsky subgrid scale turbulence model as [16,17]

$$C = \frac{L_{ij} M_{ij}}{M_{kl} M_{kl}}, \quad (4)$$

with L_{ij} and M_{ij} given as

$$L_{ij} = \hat{\bar{u}_i \bar{u}_j} - \hat{\bar{u}_i} \hat{\bar{u}_j}, \quad (5)$$

$$M_{ij} = 2\bar{\Delta}^2 |\bar{S}| \hat{\bar{S}_{ij}} - 2\bar{\Delta}^2 |\bar{S}| \hat{\bar{S}} \hat{\bar{S}_{ij}}, \quad (6)$$

where $(\hat{\cdot})$ denotes variables calculated on a test filter, which is chosen to be twice as large as the grid spacing. A box filter in the physical space based on the trapezoidal rule is used, while no filtering is implemented in the y -direction normal to the walls. The values of C are averaged over the spanwise direction and a cutoff is used to ensure nonnegative values of the total viscosity, i.e., the kinematic plus the turbulent viscosity. The quantity Π in Eq. (2) is the extra pressure gradient required to keep the mass flow rate of the air through the channel constant, and δ_{ij} is the Kronecker delta.

An immersed boundary method is utilized to treat numerically the square bars (for details see [18–20]). This technique consists of imposing zero values for all velocity components of the carrier phase on the stationary boundary surface that does not necessarily coincide with the computational grid, allowing the solution of flows over complex geometries without the need for computationally intensive body-fitted grids. At the first grid point outside each roughness element, all the viscous derivatives in the LES equations are discretized by using the distance between the fluid velocity components and the boundary of the square bars. Zero velocities are imposed on all the grid points within the roughness elements (for more details see [20]).

The time evolution of the particle-laden turbulent flows with square bars placed on one wall is obtained by solving numerically the LES Eqs. (1) and (2) based on a semi-implicit, fractional step method [20,21]. A second-order central finite differencing scheme on a Cartesian staggered grid is used for the spatial discretization. The time integration of the discretized equations consists of a combination of an explicit low storage third-order Runge–Kutta method for the non-linear convection terms and the extra subgrid stress, and an implicit second-order Crank–Nicolson method for the linear diffusion terms. The resulting system of algebraic equations is inverted by an approximate factorization technique. The Poisson equation formulated for the pseudo-pressure that is used to obtain a divergence-free velocity field is solved by fast Fourier transforms in the streamwise and spanwise directions, and tri-diagonal matrix inversion in the direction normal to the walls.

2.2. Lagrangian particle-tracking model

Once the fully developed turbulent airflow is obtained by LES, the behavior of rigid particles is simulated by integrating the equations of motion for each particle explicitly over time. The following assumptions for the Lagrangian particle-tracking model are made: (a) the particles are non-interacting, non-deformable, solid spheres that are smaller than the smallest length scales of the airflow and, thus, can be approximated as point-particles; (b) the density of the

particles is large relative to that of the carrier phase; (c) temperature and humidity effects on the particle deposition are not considered; (d) particle rebound and re-suspension are not taken into account, in order to facilitate the comparison against previous numerical studies of particle deposition onto smooth walls [22,23]; (e) the concentration of particles in the airflow is low, ensuring dilute flow conditions and, therefore, the feedback effect of particles on the turbulent airflow and the particle-particle collisions are not included in the simulations (i.e., one-way coupling); (f) drag and gravity forces are the significant forces acting on the particles, while virtual mass, pressure gradient, and Basset forces can be neglected, which is justified by the relatively high mass density ratio between the phases in the present study [24]. The lift force has also been discarded in the particle equation of motion, in order to focus on the investigation of the wall roughness effect on the particle deposition within a manageable parameter range; (g) the effect of subgrid scales on the particle motion is assumed to be negligible. This is a reasonable assumption given the filtering due to the particle inertia and the moderate Reynolds number of the present flows, for which there is a relatively weak impact of the unresolved on the resolved scales [15,25–27].

The trajectories of the particles are calculated in a Lagrangian reference frame considering the drag $f_{D,i}^n$ and gravity f_G forces. The particle equations of motion can be written as

$$\frac{dx_{p,i}^n}{dt} = u_{p,i}^n, \quad (7)$$

$$\frac{du_{p,i}^n}{dt} = \frac{f_{D,i}^n}{m_p} + \frac{f_G}{m_p} = \frac{3}{4} \frac{\rho_f}{\rho_p} \frac{c_D}{d_p} |\tilde{\mathbf{u}}_{@p}^n - \mathbf{u}_p^n| (\tilde{\mathbf{u}}_{@p,i}^n - \mathbf{u}_{p,i}^n) + g \delta_{i1}, \quad (8)$$

where $u_{p,i}^n$ and $\tilde{u}_{@p,i}^n$ are the velocity of the n particle and the undisturbed fluid velocity at the particle position $x_{p,i}^n$, respectively, m_p ($=\rho_p \pi d_p^3/6$) is the spherical particle mass, ρ_p , d_p are the particle density and diameter, respectively, and bold symbols indicate vectors. The Stokes drag force is corrected for inertial effects at non-negligible particle Reynolds numbers Re_p by the coefficient c_D given by [28]

$$c_D = \frac{24}{Re_p} (1 + 0.15 Re_p^{0.687}), \quad (9)$$

where $Re_p = |\tilde{\mathbf{u}}_{@p}^n - \mathbf{u}_p^n| d_p / v$. The particles exiting the channel domain through the planes normal to the streamwise and spanwise directions are reintroduced in it from the corresponding opposite boundary plane with their exiting velocities, while the left wall is considered to be perfectly absorbing. Deposition of particles is identified when their center is less than $d_p/2$ distance from the closest surface of the channel walls or the roughness elements. It is detected as a geometric intersection of the particle trajectory and the rough wall. In particular, the detection algorithm of particle deposition consists of the following steps:

- For each particle with initial position $x_{p,i}(t)$ (P), calculate displacement and final position $x_{p,i}(t+dt)$ (P') using Eqs. (7)–(9).
- Determine if intersection with any of the planes of the rough wall occurs (lower horizontal plane $x = X_l(nbl)$, upper horizontal plane $x = X_u(nbl)$, outer vertical plane $y = Y_{out}$, and inner vertical plane $y = Y_{in}$, where nbl is the number of the square bar). The possible combinations are summarized in Fig. 2 for a particle located at time t inside or outside the cavity with either positive or negative streamwise velocity.
- If intersection is detected during this time step, then calculate the contact time t_c ($0 < t_c \leq dt$) and the particle position $x_{pc,i}$ (x_{pc}, y_{pc}, z_{pc}) at contact with each intersection plane (I , I' , etc.).
- If the particle position $x_{pc,i}$ belongs to any of the surfaces of the rough wall (inner vertical surface: $\forall z, y_{pc} - d_p/2 = Y_{in}$ and $X_u(nbl) + d_p/2 < x_{pc} < X_l(nbl + 1) - d_p/2$; outer vertical surface: $\forall z, y_{pc} - d_p/2 = Y_{out}$ and $X_l(nbl) \leq x_{pc} \leq X_u(nbl)$; lower and upper horizontal surfaces: $\forall z, x_{pc} + d_p/2 = X_l(nbl)$ or $x_{pc} - d_p/2 = X_u(nbl)$ and $Y_{in} + d_p/2 < y_{pc} \leq Y_{out}$), then particle deposition occurs during this time step. If multiple deposition events in more than one surface are detected (for example, particles at I and I' positions in Fig. 2), the deposition event with the smallest contact time is chosen. The latter guarantees that only real events are taken into account.
- If the particle position $x_{pc,i}$ does not belong to any of the surfaces of the rough wall, then the particle does not deposit during this time step.
- If no intersection is detected during this time step, then the particle does not deposit.

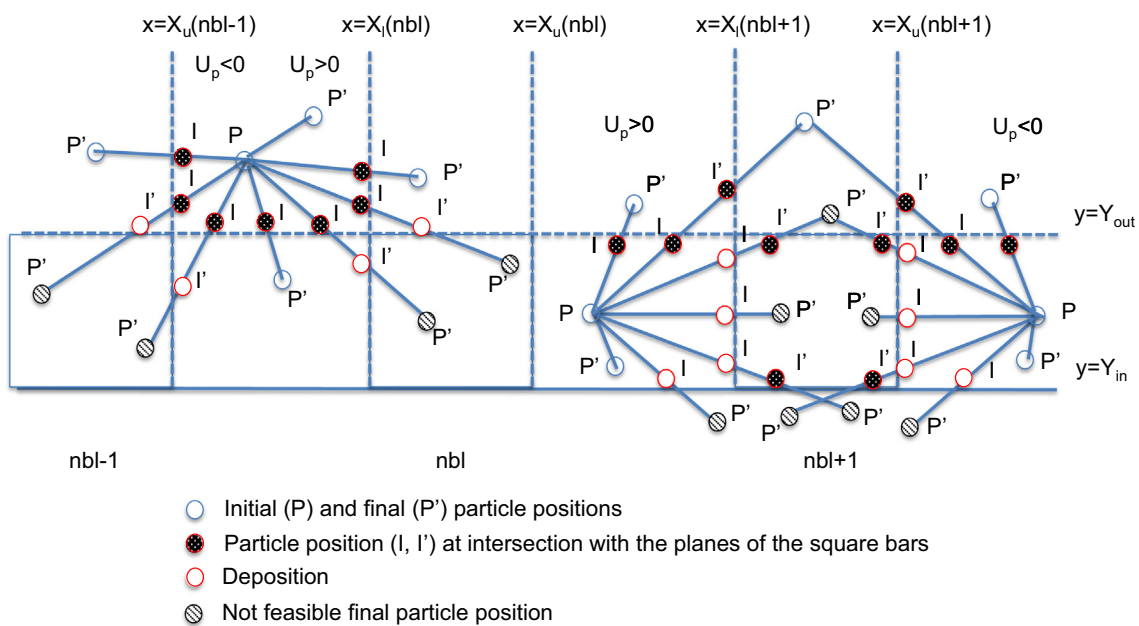


Fig. 2. Various particle trajectories near the square bars.

The exact position of a particle that deposits is computed efficiently and accurately based on the above algorithm. The intersection of the particle trajectory with any of the planes of the rough wall is determined based on the initial and final particle position. For example, for a particle with $u_p > 0$, the condition for intersection with the lower horizontal surface is simply: $x_p(t) + d_p/2 < X_l$ and $x_p(t + dt) + d_p/2 > X_l$. The contact time is computed by assuming that the distance from the plane is at least equal to its radii, e.g., $x_{pc} = X_l - d_p/2$, and that the particle velocity is constant as follows: $t_c = dt (X_l - d_p/2)/(x_p(t + dt) - x_p(t))$. If $0 < t_c \leq dt$, then the particle position at $x_{pc,i}$ ($x_{pc} = X_l - d_p/2$, y_{pc} , z_{pc}) is calculated based on Eq. (7) using t_c . Finally, if the particle position belongs to the lower horizontal surface of the rough wall, $Y_i < y_{pc} \leq Y_{out}$, then particle deposition occurs.

The positions and velocities of the particles are computed simultaneously with the numerical solution of the LES equations by performing time integration of Eqs. (7) and (8) with a second-order explicit Adams–Bashforth method. The undisturbed fluid velocity $\bar{u}_{\text{at},i}^n$ in Eq. (8) is approximated by the velocity that is obtained from the numerical solution of the LES Eqs. (1) and (2), evaluated at the particle positions using third-order Lagrange polynomials.

3. Simulations overview

All simulations are performed at the same Reynolds number of $Re (= u_b 2h/v) = 5600$ based on the bulk velocity u_b (≈ 7.8 m/s) and the distance between the right smooth wall and the crest of the left rough wall $2h$ (≈ 0.01 m). The fluid density is $\rho_f = 1.12$ kg/m³, and the fluid kinematic viscosity is $v = 0.15 \times 10^{-4}$ m²/s. The values of the ratio of the cavity width w to the dimension of the square bar k examined here are $w/k = 0$ (flat channel) and 1 (rough channel) with $k = 0.2h$ (≈ 0.001 m). The dimensions of the channel in the streamwise and spanwise directions are $L_x = 8h$ and $L_z = \pi h$, respectively, and the computational mesh is $201 \times (30 + 64) \times 65$ in the x , y , and z -directions, respectively. Each roughness element is discretized by using 30 almost equidistant grid points over the range of $-1.2 < y/h < -1$, while 5 grid points are used in the x -direction. The rest 64 grid points are unevenly distributed in $-1 < y/h < 1$. A small enough time step is guaranteed by fixing the CFL number at a constant value of 0.5.

The results presented here are grid converged as indicated in Fig. 3, which shows the influence of several computational meshes on the mean streamwise velocity \bar{U} and the root-mean-square (rms) fluid velocity fluctuations in the streamwise U_{rms} and spanwise W_{rms} directions. It is seen that the profiles using $81 \times (30 + 64) \times 65$ points do not differ largely from those using $201 \times (30 + 64) \times 65$ points. The results from the $201 \times (30 + 32) \times 65$ simulations, which use fewer points in the outer flow region in the wall-normal direction, are in generally good agreement with the results obtained by the adopted grid. The results produced based on $201 \times (15 + 64) \times 65$ points are close to those of the simulations with $201 \times (30 + 64) \times 65$ points. A poor performance is indicated in the $201 \times (30 + 64) \times 33$ simulations revealing that the refinement in z has a greater influence than that in x . The fact that the present results are grid converged is also indicated by the good agreement of the LES results for \bar{U} and U_{rms} , W_{rms} with the DNS results based on a much finer grid resolution for the turbulent channel flows without and with roughness elements (see discussion below in Section 4.1). A detailed analysis of the performance of LES, including grid sensitivity studies, and its capability to reproduce the main results and trends of the turbulent airflow in channels roughened by square bars can be found in Dritselis [20].

At first, the particle-free turbulent channel flow with smooth walls at $Re = 5600$ is simulated. Small disturbances (white noise)

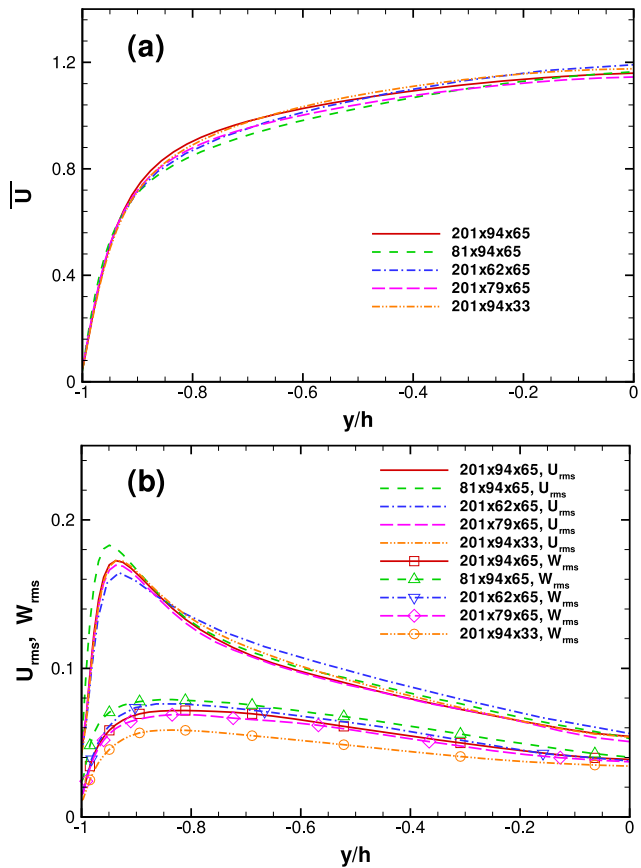


Fig. 3. Effect of grid resolution on \bar{U} (a) and U_{rms} , W_{rms} (b) made non-dimensional by the fluid bulk velocity.

with amplitude of 0.025 are imposed on a laminar Poiseuille profile, and the flow is simulated until a fully developed state is established ($T = 2000$). LES of the particle-free turbulent channel flow with $w/k = 1$ is then carried out (up to $T = 4000$), using the fully developed flow with two smooth walls as initial conditions. Next, the trajectories of 5×10^5 particles are calculated in the turbulent flow with one rough wall at $w/k = 1$, after having established that a fully developed state has been reached. Initially, the particles are introduced into the airflow in the region of $-1 < y/h < -0.7$ near the rough surface, with velocities equal to those of the carrier phase at their positions. Results are obtained for six samples of particles with non-dimensional diameters of $d_p/h \times 10^3 = 1.178$, 1.667, 2.357, 3.727, 7.454, and 10.541, and non-dimensional response times of $St^+ = \tau_p/(v/u_{\tau,0}^2) = (S_{pf} d_p^2/18v)/(v/u_{\tau,0}^2) = 2.5$, 5, 10, 25, 100, and 200, where τ_p is the particle relaxation time and $u_{\tau,0}$ is the wall friction velocity for the $w/k = 0$ case. The values of particle diameter range from 6.4 μm to 57 μm , while the particle-fluid density ratio is $S_{pf} = \rho_p/\rho_f = 1000$. A downward airflow is considered and the Froude number is $Fr = u_b^2/gh \approx 1142$.

The cases studied in this work consist of indicative particle-laden flows appropriate to assess the effect of the rough vertical surface on the particle deposition under the influence of gravity aligned in the flow direction by using a combination of adequate numerical methods. More specifically, several results and trends of the fluid flow and the dispersed particles can be reproduced satisfactorily using LES together with Lagrangian particle-tracking, such as fluid velocity statistics, Lagrangian and Eulerian statistics of the particulate phase, particle concentration and deposition, and preferential concentration (see, for example, [15,15,25–27,29,30]). The fluid flow solver (LES/immersed boundary method)

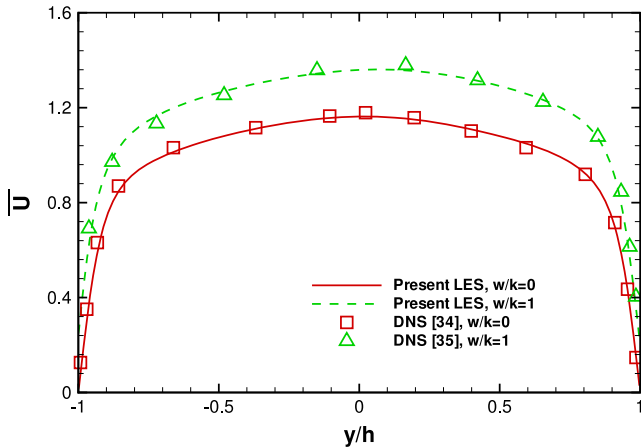


Fig. 4. Distribution of the mean streamwise velocity for the turbulent flow in a flat channel $w/k = 0$ and in a channel roughened by square bars $w/k = 1$. The results for $w/k = 1$ are shifted upwards by 0.2.

and the Lagrangian particle-tracking solver have been extensively used and successfully verified previously [2,30–33].

The run time of a typical particle-laden flow simulation using a serial version of an in-house code [21] is approximately three days. All simulations were performed in the Linux-based MPI cluster facility (2.3 GHz Intel i5/8 GB RAM nodes) of the Fluid Mechanics and Turbomachinery Laboratory, University of Thessaly.

4. Results and discussion

4.1. Turbulent airflow in smooth and ribbed channels

The accurate prediction of the turbulent airflow is essential in the study of particle deposition at smooth and rough walls. Figs. 4 and 5 show a comparison of the present results with the direct numerical simulation (DNS) data of Kim et al. [34] in the case of the turbulent flow in a flat channel. It can be seen that the LES distributions of the mean velocity in the streamwise direction \bar{U} and the rms velocity fluctuations U_{rms} , V_{rms} , W_{rms} agree closely with the DNS results. Also shown in Figs. 4 and 5 is a comparison of the LES airflow model against the DNS results of Leonardi et al. [35] in the case of a ribbed channel with $w/k = 1$. It is observed that the mean velocity yielded by LES coincides with the DNS profile. An under-prediction of the LES fluctuating velocities may be seen, but the overall agreement between the solution methods can be considered acceptable.

In simulations using RANS models, the wall-normal component V_{rms} is usually modified near the smooth wall in order to improve the predictions of particle deposition [6–9]. Fig. 3 shows also the results for the correction 1 based on the data of Kim et al. [34]

$$V_{rms} = 0.008y^{+2} \text{ for } y^+ < 4, \quad (10)$$

and the correction 2 [8]

$$V_{rms} = (0.0116y^{+2})/(1 + 0.203y^+ + 0.0014y^{+2.41}) \text{ for } y^+ < 30, \quad (11)$$

where y^+ is the non-dimensional distance given by $y^+ = yu_t/v$, and u_t is the wall friction velocity. It is seen that both corrections have similar asymptotic wall behavior, while correction 2 leads to greater values of V_{rms} for $y^+ < 30$ relative to the numerical solutions in the $w/k = 0$ case. This implies that the adoption of correction 2 in RANS simulations of the turbulent flow in a rough channel will probably enhance the fluid velocity fluctuations in the y -direction. Consequently, the wall-normal particle velocities near the square bars may also be greater than those at $w/k = 0$, increasing particle depo-

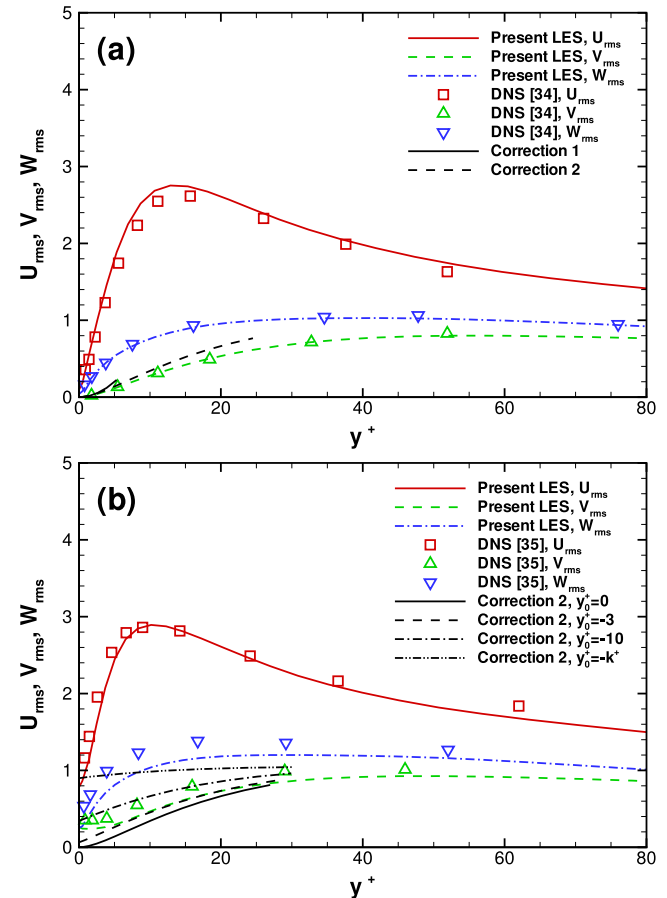


Fig. 5. Distribution of the rms velocity fluctuations for the turbulent flow in a flat channel $w/k = 0$ (a) and in channel roughened by square bars with $w/k = 1$ (b). Correction 1 (Eq. (10)) and correction 2 (Eq. (11)) are also shown for various shifts of their origin y_0^* .

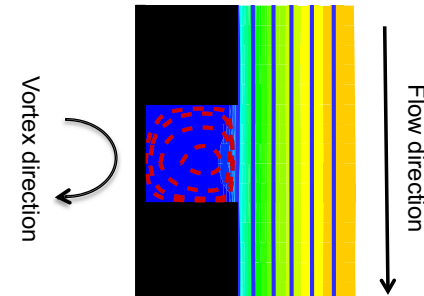


Fig. 6. Mean streamlines and contours of the mean streamwise velocity for the turbulent flow in a channel roughened by square bars with $w/k = 1$.

sition. However, it should be noticed that the behavior of the fluctuating fluid velocities near the crest of roughness elements differs significantly than that in the $w/k = 0$ case, as shown in Fig. 5. Moreover, the DNS and LES profiles of V_{rms} at $w/k = 1$ cannot be reproduced adequately by the correction 2. This is true for all distributions of correction 2 with different origins shifted by $y_0^* = 0, -3, -10$, and $-k^* \approx 34.6$ with respect to the $y/h = -1$ plane. Thus, the corrections 1 (Eq. (10)) and 2 (Eq. (11)) should be used with caution in RANS simulations of channel flows with square bars placed transversally on one wall. It is clear that new *ad hoc* corrections have to be developed that account properly for the modifications of the wall-normal velocity fluctuations of the carrier phase adjacent to the roughness elements.

The mean streamlines near the smooth wall of a fully developed turbulent flow are parallel to the wall plane. Fig. 6 shows that the cavity of the rough wall with $w/k = 1$ is populated by a single recirculation, while the mean flow pattern over the rough wall seems to be almost unaffected by the presence of the square bars. It should be noted that the LES mean streamlines for $w/k = 1$ resemble well those of the flow visualizations of Leonardi et al. [35].

The relationship between the particle deposition coefficient and the particle response time is usually employed as a measure of particle deposition rates. The quantities mentioned above are made non-dimensional using the wall friction velocity u_τ . Thus, an accurate prediction of u_τ is crucial for the proper interpretation of particle deposition results. The non-dimensional wall friction velocity $U_\tau (= u_\tau/u_b)$ can be determined as $U_\tau \equiv \tau_w^{1/2} = (f/2)^{1/2} = (P_d + F_d)^{1/2}$, where τ_w is the wall stress, f is the friction factor, P_d is the form drag, and F_d is the friction drag. The quantities F_d and P_d are calculated by integrating the viscous shear stress C_f and pressure $\langle \bar{P} \rangle_{z,t}$ obtained by LES at the rough wall over a streamwise wavelength λ , $F_d = \lambda^{-1} \int_0^\lambda C_f \mathbf{s} \cdot \mathbf{x} ds$ and $P_d = \lambda^{-1} \int_0^\lambda \langle \bar{P} \rangle_{z,t} \mathbf{n} \cdot \mathbf{x} ds$, where \mathbf{x} is the unit vector in the x -direction, s is a coordinate that follows the contour of the solid surface, \mathbf{n}, \mathbf{s} are the unit vectors normal and parallel to the wall, respectively, and $\langle \rangle_{z,t}$ denotes averaging over the z -direction and time. Obviously, u_τ depends only on F_d for a smooth wall, since it holds that $P_d \equiv 0$ at $w/k = 0$. The non-dimensional viscous shear stress is calculated as $C_f = Re^{-1} (\partial \langle \bar{U} \rangle_{z,t} / \partial Y)_{Y=\pm 1}$, where $\bar{U} = \bar{u}/u_b$ and $Y = y/h$. It is found that the non-dimensional wall friction velocity in the flat channel flow is $U_\tau = 6.11 \times 10^{-2}$, while it is increased up to $U_\tau = 6.21 \times 10^{-2}$ for the turbulent flow in the ribbed channel with repeated square bars of size $k = 0.2h$ and a spacing between them of $w = k$.

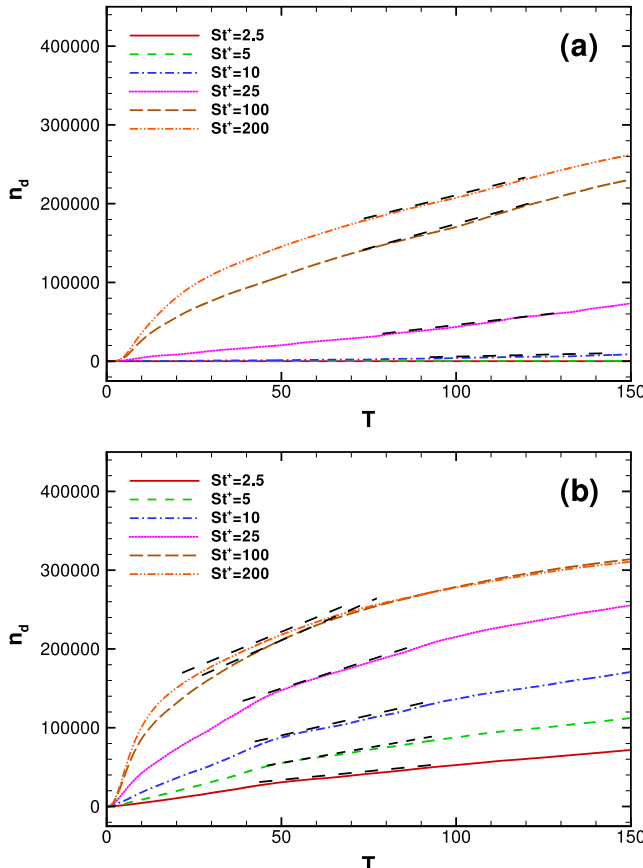


Fig. 7. Time history of the particles deposited at the smooth wall (a) and the rough wall with $w/k = 1$ (b) in the presence of gravity aligned in the flow direction.

4.2. Particle deposition

During the simulations, the particles deposit at the left vertical wall and, thus, the airflow in the channel is gradually depleted from particles. Fig. 7a and b shows the time evolution of the number of particles that deposit n_d in the cases with $w/k = 0$ and 1 , respectively, for various values of the particle response time. The general observation of Fig. 7 is that the removal of particles is more effective in the presence of square bars. It is also evident that the particles are transferred more rapidly in the region close to the rough wall. For both flows at $w/k = 0$ or 1 , higher values of n_d can be seen as the particle response time is increased. Fig. 7 shows that n_d reaches equilibrium after an initial transient time period, as indicated by the slope of the curves that approaches asymptotically a constant value as time increases. This suggests that the number of deposited particles n_d per unit time T remains roughly constant, and this value of n_d/T is used in the calculation of the particle deposition coefficient k_d . It can be observed that the slope of n_d is increased at $w/k = 1$, revealing an increase to the deposition rate due to the square bars. At longer times ($T = t u_b/h > 150$), the slope of n_d is decreased for both smooth and rough channels because a significant fraction of particles has either deposited at the wall or moved away from it.

Fig. 8 shows the variation of the normalized deposition coefficient k_d^+ ($= k_d/U_\tau$) with the non-dimensional particle response time St^+ for smooth ($w/k = 0$) and rough ($w/k = 1$) channels. The coefficient k_d is calculated as (see, for example, [23,29,33])

$$k_d = \frac{1}{A_d} (n_d/\delta t_d)/(n_{\delta V}/\delta V), \quad (12)$$

where n_d is the number of particles that deposited in a time interval of δt_d , $n_{\delta V}$ is the total number of particles located initially within a region of l distance from the vertical crests of the rough wall with volume $\delta V = l L_x L_z + 20k w L_z$, and A_d is the deposition area given by $A_d = L_x L_z + 40k L_z$. The LES predictions of the deposition coefficient corresponding to the air-particle flows in a vertical flat channel with $w/k = 0$ are in close agreement with previous numerical and experimental observations. For example, k_d^+ is increased for particles having response times in the diffusion/impaction regime $2.5 \leq St^+ \leq 25$. Moreover, it obtains an approximately constant value in the inertia-moderate region with high values of St^+ . High inertia particles perform an almost ballistic motion, they are capable of acquiring sufficient momentum to coast the viscous sublayer and they deposit by impaction at the smooth wall. In contrast,

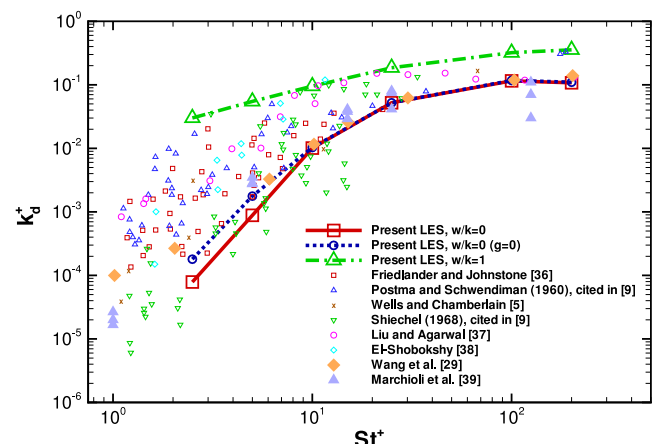


Fig. 8. Particle deposition coefficient k_d^+ as a function of the non-dimensional particle response time St^+ for the turbulent flow in a flat channel and in a channel roughened by square bars with $w/k = 1$ in the presence of gravity aligned in the flow direction.

low St^+ particles may reside in the vicinity of the smooth wall for long time periods before they deposit due to the influence of small turbulent fluctuations of the carrier phase. Particles with intermediate values of St^+ may deposit by either direct impaction or turbulent diffusion, as a consequence of their interactions with coherent structures in the turbulent fluid flow [22,23].

Fig. 8 also shows data of the particle deposition coefficient from several experiments collected by [14] and other experimental measurements [5,36–38], as well as from representative numerical studies [29,39]. A very large spread in the values of k_d^+ is obvious, owing to differences between the experiments, as for example, in the Reynolds number, the density ratio between the two phases, the particle response time, the gravity orientation, and the Froude number. The present LES predictions of k_d^+ at $w/k = 0$ are in good agreement with the LES results of Wang et al. [29], under the same numerical conditions and similar parameters in the absence of gravity ($g = 0$), while the agreement is acceptable with the DNS results of Marchioli et al. [39], when the differences in the Reynolds number and the particle parameter space are considered.

The particle deposition coefficient is raised in the turbulent flow at a channel roughened by square bars placed transversally on the wall as indicated in Fig. 8. The variation of k_d^+ with St^+ at $w/k = 1$ is similar to that observed at $w/k = 0$. However, a weaker dependence of k_d^+ on St^+ is noticeable in the former case. More specifically, k_d^+ is increased approximately from 10^{-2} to 10^{-1} for $2.5 \leq St^+ \leq 25$, while it saturates as St^+ is increased further. The largest value of k_d^+ at $w/k = 1$ corresponds to the case with particles having $St^+ = 200$. The augmentation of the deposition coefficient in the air-particle flows inside a vertical channel with roughness elements is consistent with previous findings [2–5,39].

4.3. Enhancement and efficiency of particle deposition

To gain further insight into the enhancement of particle deposition due to the rough wall, a comparison between the numerical predictions of k_d^+ in the cases with $w/k = 0$ and 1 is performed. The deposition coefficient is increased from about 8×10^{-5} at $w/k = 0$ to approximately 3×10^{-2} at $w/k = 1$ for low inertia particles, revealing an augmentation in k_d^+ of three orders of magnitude. On the other hand, k_d^+ is increased from 10^{-1} at $w/k = 0$ to 0.3 at $w/k = 1$ for high inertia particles. In order to quantify properly the above observations, the enhancement ratio of particle deposition γ is calculated as

$$\gamma = \frac{(k_d^+)_\text{smooth}}{(k_d^+)_\text{rough}}, \quad (13)$$

and shown in Fig. 9. It can be seen that γ is approximately 400 for particles with $St^+ = 2.5$ and it is decreased down to $\gamma \approx 3$ with increasing particle response time up to $St^+ = 100$, while it is slightly increased for $St^+ = 200$. Consequently, the use of a rough surface consisting of square bars placed perpendicularly to the flow direction can lead to a significant augmentation of particle deposition for small size particles with $d_p \approx 6 \mu\text{m}$, while the enhancement is reduced for larger particles with $d_p \approx 60 \mu\text{m}$, as compared with the deposition of particles occurring at smooth walls.

The performance of the present rib-roughened layout is also examined with respect to the achievement of the maximum possible particle deposition with the minimum pressure and friction losses. For this reason, the friction-weighted enhancement ratio η of particle deposition defined as [2]

$$\eta = \frac{(k_d^+)_\text{rough}/(k_d^+)_\text{smooth}}{(f_\text{rough}/f_\text{smooth})^{1/3}}, \quad (14)$$

was calculated and also shown in Fig. 9. The efficiency ratio η can be considered a comparison measure of the particle deposition coeffi-

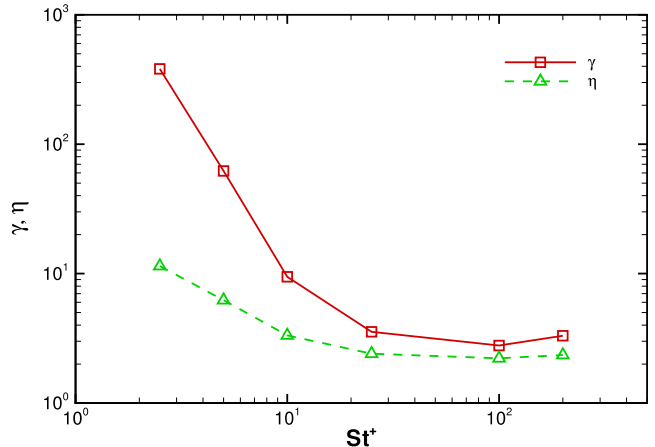


Fig. 9. Enhancement ratio γ and efficiency ratio η of the particle deposition as a function of the non-dimensional particle response time St^+ .

cient between the flows in the rough and smooth channels under the same fan power. The quantities k_d^+ and f can be calculated easily and accurately using the LES data. The friction factor ratio of the rough to the smooth channel $f_\text{rough}/f_\text{smooth}$ was computed to be 2.066 at $w/k = 1$ in the present work. Fig. 9 indicates that the efficiency ratio is higher than unity for all particle ensembles examined here, suggesting that the ribbed channel configuration effectively enhances particle deposition, while the increase of energy losses is kept relatively low. This is more obvious for the small size particles for which η is about 10, while for the larger particles it is about 2.5. The dependence of η on the particle response time is similar to that discussed previously for γ , since the ratio $f_\text{rough}/f_\text{smooth}$ does not vary with St^+ in the present one-way coupling simulations.

Fig. 10 shows the effect of the rough wall on the mean wall-impact particle velocity components $V_{p,d}$, $U_{p,d}$, and $W_{p,d}$ in the wall-normal, streamwise, and spanwise directions, respectively, conditionally averaged over all depositing particles. In particular, Fig. 10a reveals that the magnitude of $V_{p,d}$ is increased at $w/k = 1$ relative to the $w/k = 0$ case, and this trend becomes stronger as St^+ is increased. Fig. 10b shows that $U_{p,d}$ is augmented for particles with high response times as compared to the flow with $w/k = 0$, while the opposite is true for low response time particles. In contrast to the $U_{p,d}$ and $V_{p,d}$ components, Fig. 10c indicates that $W_{p,d}$ remains almost constant with the variation of St^+ at $w/k = 1$. The motion of non-colliding particles is at equilibrium with the underlying fluid motions and, thus, any change in the airflow because of the square bars is reflected on the dynamic particle behavior. The influence of the neighboring fluid motions on the particle trajectory becomes less significant as the particle response time increases due to the particle inertia that filters out high frequencies and small scales of the fluid flow. The observed increase of $V_{p,d}$ points out that the particles can coast rather freely the region adjacent to the rough wall with $w/k = 1$, thus, favoring deposition by direct impaction. Since the airflow over the roughness elements is little affected as demonstrated in Fig. 6, it is also expected that turbulent diffusion will continue to have an important role in the deposition of particles at the rough surface with $w/k = 1$, in a similar manner as in smooth walls [26,32,39].

In the case of rough walls, there are two additional mechanisms of particle deposition: the augmentation of the effective deposition area and the interception mechanism. For square bars with $w/k = 1$, the deposition area is two times greater than that for the smooth wall. The interception mechanism is the consequence of the inability of particles to follow exactly the surrounding fluid motions because of their inertia. Consequently, the particles will probably end up colliding onto the frontal surface of the protruding square

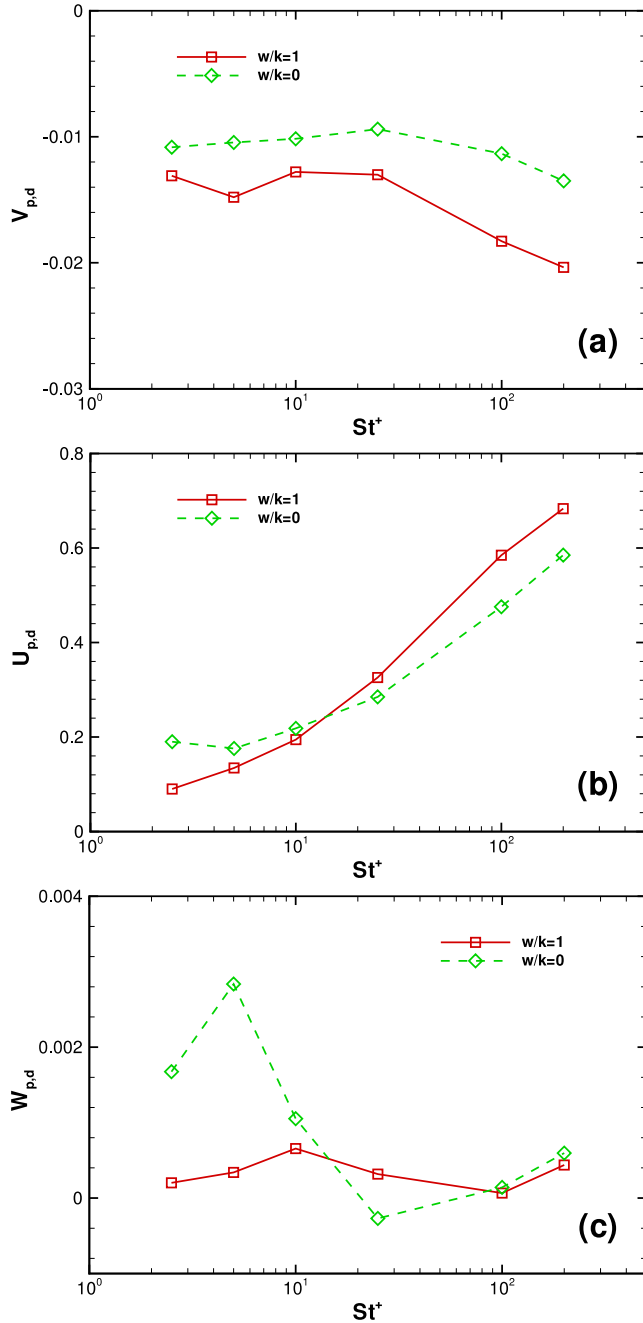


Fig. 10. Variation of the mean wall-impact velocity in the wall-normal $V_{p,d}$ (a), streamwise $U_{p,d}$ (b), and spanwise $W_{p,d}$ directions (c) with the non-dimensional particle response time St^+ .

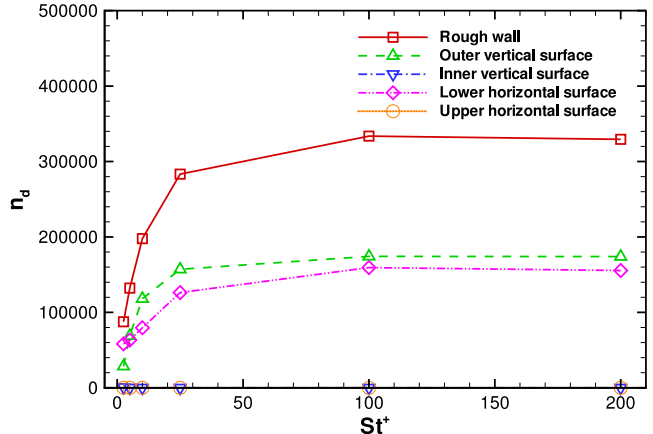


Fig. 11. Variation of the number of particles deposited n_d at the rough wall with $w/k = 1$, the outer vertical surface (DE), the inner vertical surface (BC), the lower horizontal surface (CD), and the upper horizontal surface (AB) with the non-dimensional particle response time St^+ .

the interception mechanism is less effective for small spacings between the square bars, in contrast to its profound predominance at higher values of w/k [4,14,16]. The fraction of particles deposited at the rear surface of the square bars (AB) is very small relative to the other surfaces of the rough wall, indicating that particle motion inside the cavities is not significantly altered by the presence of local recirculations. In contrast, the secondary flows seem mainly to modify the structures adjacent to the square bars [19,20,35], leading to a weaker resistance as the particles are transferred near the roughness elements. Consequently, each surface of the rough wall does not contribute the same amount to the increase of particle deposition.

5. Conclusions

In this study, the particle deposition at a vertical wall consisting of protruding square bars was investigated using LES of a downward turbulent flow in a ribbed channel at $Re = 5600$ together with Lagrangian particle-tracking. The relative height of the square bars with respect to the half distance of the channel walls was $k/h = 0.2$ and the spacing between two successive roughness elements was $w = k$. The trajectories of six particle ensembles having non-dimensional response times $St^+ = 2.5, 5, 10, 25, 100$, and 200 were tracked in the presence of gravity aligned in the flow direction with Froude number $Fr = 1142$. The following main conclusions can be drawn:

1. A significant enhancement of the particle deposition takes place in the turbulent flows at $w/k = 1$. The particle deposition coefficient exhibits a weaker dependence on the variation of particle response time as compared with the $w/k = 0$ case.
2. The enhancement ratio was found to be approximately $\gamma \approx 400$ for small size particles with $St^+ = 2.5$, while it is decreased down to $\gamma \approx 3$ for larger particles with $St^+ = 100$ and 200 . The friction-weighted enhancement ratio of the particle deposition was estimated to be greater than unity for all particle ensembles examined here, indicating that the present ribbed channel configuration is an energy efficient alternative method of increasing particle deposition.
3. The changes in the airflow by the presence of the square bars are reflected on the dynamic behavior of the suspended particles, leading to a significant increase of deposition by impaction. Deposition due to interception was found to be of similar importance. In contrast, few particles were deposited at the rear surface of the square bars.

bars rather than surpassing them (see, for example, [40]). In order to quantify the significance of the various mechanisms, the number of particles deposited at each surface of the rough wall was monitored during the simulations and it is shown in Fig. 11 at time $T = 200$ after the release of particles into the fully developed airflow. It is clear that the enhancement of particle deposition at $w/k = 1$ is closely related to the direct impaction of particles at the outer vertical surface and the frontal surface of the roughness elements. It is seen that the deposition due to interception, as this indicated by n_d at the lower horizontal surface (CD), is equally important as the deposition by inertial impaction that takes place at the outer vertical surface of the rough wall (DE). It turns out that

Acknowledgments

Partial financial support from the Mechanical Engineering Department of the University of Thessaly and from the Association EURATOM–Hellenic Republic during 2008–2016 is gratefully acknowledged. The content of this paper is the sole responsibility of its author and it does not necessarily represent the views of the European Commission or its services.

References

- [1] Y.J. Suh, S.S. Kim, Effect of obstructions on the particle collection efficiency in a two-stage electrostatic precipitator, *J. Aerosol. Sci.* 27 (1996) 61–74.
- [2] A.C.K. Lai, M.A. Byrne, A.J.H. Goddard, Measured deposition of aerosol particles on a two-dimensional ribbed surface in a turbulent duct flow, *J. Aerosol. Sci.* 30 (1999) 1201–1214.
- [3] A.C.K. Lai, M.A. Byrne, A.J.H. Goddard, Aerosol deposition in turbulent channel flow on a regular array of three-dimensional roughness elements, *J. Aerosol. Sci.* 32 (2001) 121–137.
- [4] A.C.K. Lai, M.A. Byrne, A.J.H. Goddard, Particle deposition in ventilation duct onto three-dimensional roughness, *Build. Environ.* 35 (2002) 939–945.
- [5] A.C. Wells, A.C. Chamberlain, Transport of small particles to vertical surfaces, *Brit. J. Appl. Phys.* 18 (1967) 1793–1799.
- [6] A. Li, G. Ahmadi, Computer simulation of deposition of aerosols in a turbulent channel flow with rough walls, *Aerosol. Sci. Technol.* 18 (1993) 11–24.
- [7] A. Li, G. Ahmadi, R.G. Bayer, M.A. Gaynes, Aerosol particle deposition in an obstructed turbulent duct flow, *J. Aerosol. Sci.* 25 (1994) 91–112.
- [8] G. Lericain, S. Drapeau-Martin, T. Barth, U. Hampel, Numerical simulation of multilayer deposition in an obstructed channel flow, *Adv. Powder Technol.* 25 (2014) 310–320.
- [9] H. Lu, L. Lu, Numerical investigation on particle deposition enhancement in duct air flow by ribbed wall, *Build. Environ.* 85 (2015) 61–72.
- [10] M. Rahimi-Gorji, T.B. Gorji, M. Gorji-Bandpy, Details of regional particle deposition and airflow structures in a realistic model of human tracheobronchial airways: two-phase flow simulation, *Comput. Biol. Med.* 74 (2016) 1–17.
- [11] M. Rahimi-Gorji, O. Pourmehran, M. Gorji-Bandpy, T.B. Gorji, CFD simulation of airflow behavior and particle transport and deposition in different breathing conditions through the realistic model of human airways, *J. Mol. Liq.* 209 (2015) 121–133.
- [12] A.R. Lambert, P. O'Shaughnessy, M.H. Tawhai, E.A. Hoffman, C.L. Lin, Regional deposition of particles in an image-based airway model: large-eddy simulation and left-right lung ventilation asymmetry, *Aerosol. Sci. Technol.* 45 (2011) 11–25.
- [13] G. Lo Iacono, P.G. Tucker, A.M. Reynolds, Predictions for particle deposition from LES of ribbed channel flow, *Int. J. Heat Fluid Flow* 26 (2005) 558–568.
- [14] G. Lo Iacono, A.M. Reynolds, P.G. Tucker, Particle deposition onto rough surfaces, *AMSE J. Fluids Eng.* 130 (2008) 074501, 1–5.
- [15] M.A.I. Khan, X.Y. Luo, F.C.G.A. Nicolleau, P.G. Tucker, G. Lo Iacono, Effects of LES sub-grid flow structure on particle deposition in a plane channel with ribbed wall, *Int. J. Numer. Meth. Biomed. Eng.* 26 (2010) 999–1015.
- [16] M. Germano, U. Piomelli, P. Moin, W.H. Cabot, A dynamic subgrid-scale eddy viscosity model, *Phys. Fluids A* 3 (1991) 1760–1765.
- [17] D.K. Lilly, A proposed modification of the Germano subgrid-scale closure method, *Phys. Fluids A* 4 (1991) 633–635.
- [18] E.A. Fadlun, R. Verzicco, P. Orlandi, J. Mohd-Yusof, Combined immersed boundary finite-difference methods for three-dimensional complex flow simulations, *J. Comput. Phys.* 161 (2000) 35–60.
- [19] P. Orlandi, S. Leonardi, DNS of turbulent channel flow with two- and three-dimensional roughness, *J. Turbul.* 7 (2006) 1–22.
- [20] C.D. Dritselis, Large eddy simulation of turbulent channel flow with transverse roughness elements on one wall, *Int. J. Heat Fluid Flow* 50 (2014) 225–239.
- [21] P. Orlandi, *Fluid Flow Phenomena: A Numerical Toolkit*, Kluwer, Dordrecht, 2000.
- [22] J.B. McLaughlin, Aerosol particle deposition in numerically simulated channel flow, *Phys. Fluids A* 1 (1989) 1211–1224.
- [23] H. Zhang, G. Ahmadi, Aerosol particle transport and deposition in vertical and horizontal turbulent duct flows, *J. Fluid Mech.* 406 (2000) 55–80.
- [24] V. Armenio, V. Fiorotto, The importance of the forces acting on particles in turbulent flows, *Phys. Fluids* 13 (2001) 2437–2440.
- [25] V. Armenio, U. Piomelli, V. Fiorotto, Effect of the subgrid scales on particle motion, *Phys. Fluids* 11 (1999) 3030–3042.
- [26] Y. Yamamoto, M. Potthoff, T. Tanaka, T. Kajishima, Y. Tsuji, Large eddy simulation of turbulent gas-particle flow in a vertical channel: effect of considering inter-particle collisions, *J. Fluid Mech.* 442 (2001) 303–334.
- [27] M.W. Vance, K.D. Squires, O. Simonin, Properties of the particle velocity field in gas-solid turbulent channel flow, *Phys. Fluids* 18 (2006) 063302.
- [28] R. Clift, J.R. Grace, M.E. Weber, *Bubbles, Drops and Particles*, Academic Press, NY, 1978.
- [29] Q. Wang, K.D. Squires, M. Chen, J.B. McLaughlin, On the role of the lift force in turbulence simulation of particle deposition, *Int. J. Multiphase Flow* 23 (1997) 749–763.
- [30] C.D. Dritselis, N.S. Vlachos, Large eddy simulation of gas-particle turbulent channel flow with momentum exchange between the phases, *Int. J. Multiphase Flow* 37 (2011) 706–721.
- [31] C.D. Dritselis, N.S. Vlachos, Numerical study of educed coherent structures in the near-wall region of a particle-laden channel flow, *Phys. Fluids* 20 (2008) 055103.
- [32] C.D. Dritselis, N.S. Vlachos, Numerical investigation of momentum exchange between particles and coherent structures in low Re turbulent channel flow, *Phys. Fluids* 23 (2011) 025103.
- [33] C.D. Dritselis, I.E. Sarris, D.K. Fidaris, N.S. Vlachos, Transport and deposition of neutral particles in magnetohydrodynamic turbulent channel flows at low magnetic Reynolds numbers, *Int. J. Heat Fluid Flow* 32 (2011) 365–777.
- [34] J. Kim, P. Moin, R. Moser, Turbulence statistics in fully developed channel flow at low Reynolds number, *J. Fluid Mech.* 177 (1987) 136–166.
- [35] S. Leonardi, P. Orlandi, R.J. Smalley, L. Djenidi, R.A. Antonia, Direct numerical simulations of turbulent channel flow with transverse square bars on the wall, *J. Fluid Mech.* 491 (2003) 229–238.
- [36] S.K. Friedlander, H.F. Johnstone, Deposition of suspended particles from turbulent gas streams, *Ind. Eng. Chem.* 49 (1957) 1151–1156.
- [37] B.Y. Liu, J.K. Agarwal, Experimental observation of aerosol deposition in turbulent flow, *J. Aerosol Sci.* 5 (1974) 145–148.
- [38] M.S. El-Shobokshy, Experimental measurements of aerosol deposition to smooth and rough surfaces, *Atmos. Environ.* 17 (1983) 639–644.
- [39] C. Marchioli, M. Picciotto, A. Soldati, Influence of gravity and lift on particle velocity statistics and transfer rates in turbulent vertical channel flow, *Int. J. Multiphase Flow* 33 (2007) 227–251.
- [40] J.H. Vincent, W. Humphries, The collection of airborne dusts by bluff bodies, *Chem. Eng. Sci.* 33 (1978) 1147–1155.